Inorganic Chemistry

Article

pubs.acs.org/IC

Hydrogenation-Induced Structure and Property Changes in the Rare-Earth Metal Gallide NdGa: Evolution of a $[GaH]^{2-}$ Polyanion Containing Peierls-like Ga−H Chains

Jonas Ångström,[†] Robert Johansson,[‡] Tapati Sarkar,[§] Magnus H. Sørby,[∥] Claudia Zlotea,[⊥] Mikael S. Andersson,[§] Per Nordblad,[§] Ralph H. Scheicher,[‡] Ulrich Häussermann,*[,#] and Martin Sahlberg[†]

[†]Department of Chemistry, Uppsala University, Box 523, SE-75120 Uppsala, Sweden

[‡]Department Physics and Astronomy, Uppsala University, Box 516, SE-75120 Uppsala, Sweden

[§]Department of Engineering Sciences, Uppsala University, Box 534, SE-75121 Uppsala, Sweden

[∥]Physics Department, Institute for Energy Technology, P.O. Box 40, NO-2027 Kjeller, Norway

[⊥]Institut de Chimie et des Matériaux de Paris-Est, CNRS-UPEC, 2-8 rue Henri Dunant, F-94320 Thiais, France

[#]Department of Materials and Environmental Chemistry, Stockholm University, SE-10691 Stockholm, Sweden

Supporting Information

ABSTRACT: The hydride $NdGaH_{1+x}$ ($x \approx 0.66$) and its deuterized analogue were obtained by sintering the Zintl phase NdGa with the CrB structure in a hydrogen atmosphere at pressures of 10−20 bar and temperatures near 300 °C. The system $NdGa/NdGaH_{1+x}$ exhibits reversible H storage capability. H uptake and release were investigated by kinetic absorption measurements and thermal desorption mass spectroscopy, which showed a maximum H concentration corresponding to "$NdGaH_2$" (0.93 wt % H) and a two-step desorption process, respectively. The crystal structure of $NdGaH_{1+x}$ was characterized by neutron diffraction ($P2_1/m$, a = 4.1103(7), b = 4.1662(7), c = 6.464(1) Å, β = 108.61(1)° Z = 2). H incorporates in NdGa by occupying two distinct positions, H1 and H2. H1 is coordinated in a tetrahedral fashion by Nd atoms. The H2 position displays flexible occupancy, and H2 atoms attain a trigonal bipyramidal coordination by centering a triangle of Nd atoms and bridging two Ga atoms. The phase stability and electronic structure of $NdGaH_{1+x}$ were analyzed by first-principles DFT calculations. NdGaH1H2 ($NdGaH_2$) may be expressed as $Nd^{3+}(H1^-)[GaH2]^{2-}$. The two-dimensional polyanion $[GaH]^{2-}$ features linear −H−Ga−H−Ga− chains with alternating short (1.8 Å) and long (2.4 Å) Ga−H distances, which resembles a Peierls distortion. H2 deficiency (x < 1) results in the fragmentation of chains. For x = 0.66 arrangements with five-atom moieties, Ga−H−Ga−H−Ga are energetically most favorable. From magnetic measurements, the Curie−Weiss constant and effective magnetic moment of $NdGaH_{1.66}$ were obtained. The former indicates antiferromagnetic interactions, and the latter attains a value of ∼3.6 μ_B, which is typical for compounds containing Nd^{3+} ions.

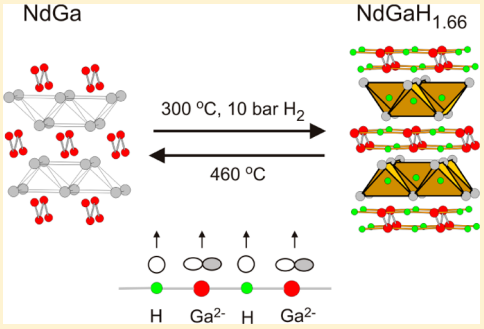

I. INTRODUCTION

Among the many intermetallic compounds that react with hydrogen, Zintl phases, made up of an active metal (i.e., alkali, alkaline earth, or rare earth) and a more electronegative p-block element, take a special role. As a characteristic feature of Zintl phases, atoms of the electronegative component appear reduced and typically form polyanionic structures to achieve an octet. Hydrogen takes an ambivalent role and can be incorporated in two principal ways: either hydridic, where H is exclusively coordinated by active metals (interstitial hydrides), or as part of the polyanion where it acts as a covalently bonded ligand (polyanionic hydrides).[1,2] The H content of hydrogenous Zintl phases is comparatively low; however, chemical structures and physical properties can change profoundly upon H incorporation.

In this Article, we report on the hydrogenation behavior of NdGa. With a few exceptions (Pm, Eu, Yb), all rare earth (RE) metals (Sc, Y, and lanthanides) form monogallides REGa, which all crystallize with the CrB structure featuring linear zigzag chains of Ga atoms (Figure 1).[3−5] According to the Zintl concept and assuming trivalent RE, Ga will correspond to Ga^{3-}; that is, the electron count per chain atom is six. The perception is then that the chain is built from singly bonded Ga species, each carrying two lone pairs (Figure 1b). The REGa compounds display interesting magnetic properties, and some systems have recently attracted attention as magnetocalorics.[6−11] In general, the compounds REGa are ferromagnets. Across the series, the Curie temperature T_c increases from 32 K

Received: October 27, 2015
Published: December 15, 2015

DOI: 10.1021/acs.inorgchem.5b02485
Inorg. Chem. 2016, 55, 345−352

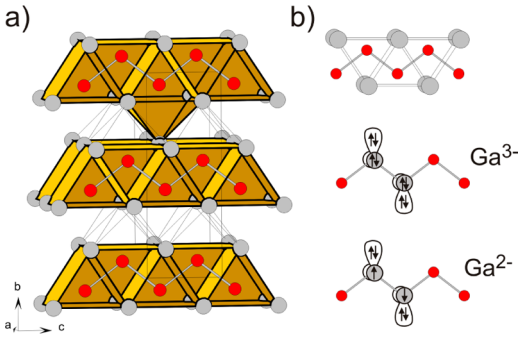

Figure 1. (a) *Cmcm* CrB-type structure of NdGa. Nd and Ga atoms are depicted as gray and red circles, respectively. The structure is built from slabs of trigonal prisms formed by the Nd atoms. Ga atoms form linear zigzag chains, and each Ga atom is surrounded by a monocapped trigonal prism of Nd atoms (one is highlighted). (b) Bonding picture of the Ga zigzag chain according to the Zintl concept. Oxidation of the polyanionic chain upon interstitial hydride formation may result in π bonding.

for PrGa to a maximum of 183 K for GdGa and then decreases to 15 K for TmGa.[12−14] For NdGa, T_c is around 50 K.[15,16] The ferromagnetic properties of REGa must be a consequence of the coupling of magnetic moments arising from localized 4f electrons, which is mediated via conduction electrons. This, on the other hand, contradicts the simple picture obtained from the Zintl concept, because electron precise singly bonded chains according to $RE^{3+}Ga^{3-}$ would not leave any excess electrons for mediating ferromagnetic coupling.

Hydrogen incorporation could give a unique possibility to probe the electronic structure of REGa systems and provide insight into the interplay between chemical bonding in the polyanion and magnetic properties. In particular, itinerant electrons may be localized as H^- through the formation of interstitial hydrides. This should be expressed in a change of the strength and possibly also the sign of the magnetic interaction. In addition, interstitial hydride formation can lead to the oxidation of the polyanion. The zigzag chain may respond to oxidation by developing π-bonding (cf., Figure 1b) or interchain bonds. The latter scenario has been observed with isoelectronic CaSi, which upon hydrogenation forms the interstitial hydride CaSiH with a new polyanionic moiety featuring three-bonded Si species.[17−19] We find that the response of NdGa to hydrogenation is rather different: H uptake beyond the composition NdGaH transforms the Ga zigzag chain into a novel two-dimensional (2D) Ga−H polyanion. At the same time, the magnetic interaction, as measured by the Curie−Weiss temperature, changes from ferromagnetic to antiferromagnetic nature.

II. METHODS

1. Synthesis. NdGa was synthesized by melting stoichiometric amounts of high-purity Nd (99.95% pure, Rare Earth Materials) and Ga (99.99%, Goodfellow) in an arc furnace. Sample batches corresponded to 5−10 g total mass. The O_2 concentration in the chamber was minimized by flushing three times with high-purity Ar and by melting a Ti-getter. To ensure homogeneity, samples were remelted five times and flipped between each melting. The total mass loss was less than 1%. Arc-melted NdGa samples were then heat-treated at 855 °C in an evacuated fused silica ampule for 20 days and subsequently ground for hydrogenation experiments. $NdGaH_{1+x}$ and its deuteride analogue were produced by heating NdGa to 300 °C at a rate of 4.5 °C/min in an autoclave that was pressurized to 10−20 bar with H_2 (D_2), followed by equilibration (up to 48 h) and cooling to room temperature. Prior to hydrogenation, the autoclave was evacuated and flushed with H_2 (D_2) three times. NdGa and its hydrides were handled in air without any noticeable change.

Powder X-ray diffraction (PXRD) patterns of NdGa, $NdGaH_{1+x}$, and $NdGaD_{1+x}$ samples were recorded on a Bruker D8 Advance diffractometer (Cu K_α radiation, λ = 1.54056 Å) equipped with a Lynxeye energy dispersive detector. Lattice parameters were determined by least-squares refinement of expected Bragg peak positions against positions extracted from the PXRD patterns.[20]

To investigate the maximum hydrogen uptake of NdGa, a kinetic absorption measurement was performed using a Setaram PCTPro -2000 volumetric instrument. NdGa sample was loaded in the reaction vessel of the apparatus. The sample was heated to 302 °C and subjected to 21 bar hydrogen gas (99.999% purity) in a vessel (known volume). Pressure was monitored until equilibrium was reached. The change in pressure was used to calculate the amount of absorbed hydrogen.

2. Structural Characterization of NdGa and $NdGaD_{1+x}$. Neutron powder diffraction patterns of NdGa and $NdGaD_x$ samples were recorded on the PUS diffractometer[21] at the JEEP II reactor of the Insitute of Energy Technology in Kjeller, Norway, using monochromatic neutron radiation with λ = 1.554 Å. The Rietveld method implemented in the FullProf program was used for structure determination and phase analysis.[22] The D atom sites were located using the GFourier routine in FullProf.[23] The peaks of the main phases were fitted using a Pseudo-Voigt peak function and the background to a linear interpolation of a set of points. In addition to the main phases, the patterns contained additional peaks, which could be explained by $NdGa_2$ (both patterns), Nd_3Ga (both patterns), and NdD_2 (the $NdGaD_x$ sample pattern). Thirteen parameters were determined for the NdGa phase from the neutron pattern: two fractional coordinates, two isotropic atomic displacement factors, three fwhm parameters, two shape parameters, the scale factor, and the *a*, *b*, and *c* lattice parameters. Thirty parameters were determined for the $NdGaD_x$ phase from the neutron patterns: eight fractional coordinates, three isotropic structure parameters, and two anisotropic structure parameters for the D2 atom, the occupancy of the D2 atom, three fwhm parameters, two shape parameters, the scale factor, and the *a*, *b*, *c*, and β lattice parameters.

3. Thermal Desorption Mass Spectroscopy of $NdGaD_{1+x}$. Desorption kinetics was studied using thermal desorption mass spectroscopy (TDS). ∼10 mg of $NdGaD_x$ sample was heated with a constant rate in high vacuum (∼1 mPa) to 600 °C during 1−8 h. The temperature of the sample was monitored using a thermocouple and the partial pressure of D_2 using a Microvision Plus residual-gas analyzer/mass spectrometer. A number of m/e signals were recorded. The m/e = 4 signal representing D_2 was used for Kissinger analysis. Activation energies (E_a) were calculated using the Kissinger equation:[24]

$$E_a = \partial(\ln(\beta/T^2_{max}))/\partial(-(RT_{max})^{-1})$$

where β is the heating rate, T_{max} is the temperature at maximum partial pressure (assumed to be the temperature at maximum reaction rate), and *R* is the ideal gas constant.

4. Computations. The theoretical calculations of the electronic structure and total energies of NdGa and structure models for $NdGaH_{1+x}$ ($0 \le x \le 1$) were performed using the first-principles all-electron projector augmented waves (PAW) method[25,26] within the Vienna Ab initio Simulation Package (VASP).[27,28] Exchange-correlation effects were treated within the generalized gradient approximation (GGA) via the Perdew−Burke−Ernzerhof parametrization.[29] A conjugate gradient algorithm was used to relax the atomic nuclei positions to a local minimum in the total energy landscape. Structure relaxations for $NdGaH_{1+x}$ did not employ any symmetry restrictions. The findsym program[30] was used to check for symmetry of atom arrangements after relaxations. Forces were converged to better than 10^{-3} eV/Å. The plane wave basis set was terminated at a kinetic energy cutoff of 600 eV. Partial occupancy of hydrogen was accounted for in a 3 × 1 × 1 supercell based on the orthorhombic CrB

DOI: 10.1021/acs.inorgchem.5b02485
Inorg. Chem. 2016, 55, 345−352

type structure with $Z = 12$ and considering the compositions $NdGaH_{1.33}$, $NdGaH_{1.50}$, $NdGaH_{1.66}$, and $NdGaH_2$. The number of calculations of random H distributions was large enough so that convergence was reached in the total energy; that is, adding more calculations of random distributions made an insignificant difference to the mean total energy. Formation energies ΔE, referring to zero kelvin, were calculated according to

$$\Delta E = 1/(x+1)[(E(NdGaH_{1+x}) - E(NdGa) - (x+1)/2\, E(H_2)]$$
$$(0 \le x \le 1)$$

where E denotes the total energy of the enclosed-in-brackets system. For the H_2 molecule, a box of $8 \times 8 \times 8$ Å^3 dimensions was used with Γ-point sampling of the Brillouin zone. Electronic structure calculations for single unit cell ($Z = 4$) NdGa, NdGaH, and $NdGaH_2$ used a grid of $21 \times 7 \times 21$ k-points to sample the Brillouin zone.[31] The decomposition of the density of state (DOS) into atomic contributions was based on spheres with radii Nd = 1.8 Å, Ga = 1.4 Å, and H = 1.1 Å. Atomic charges were calculated using Bader analysis.[32,33] NdGa was treated as nonmagnetic, and calculations were thus non spin-polarized.

5. Magnetic Measurements. Magnetization measurements were performed as a function of temperature using a Quantum Design MPMS SQUID magnetometer. M versus T measurements were done both at low field ($H = 0.005$ T) to determine the transition temperature of the samples, as well as in high field ($H = 0.1$ T) to do a Curie–Weiss fit and estimate the effective magnetic moment (μ_{eff}) and Curie–Weiss temperature (Θ_{CW}) of the samples. M versus H measurements were performed at 6 K in the field range of ±5 T to determine the saturation magnetization as well as to study the field dependence of the samples.

III. RESULTS AND DISCUSSION

A. Hydrogen Sorption and Desorption Behavior of NdGa. Initially NdGa readily absorbs hydrogen. The kinetic absorption experiment performed at 300 °C (shown in Figure 2) revealed an uptake corresponding to 1.15 H/formula unit

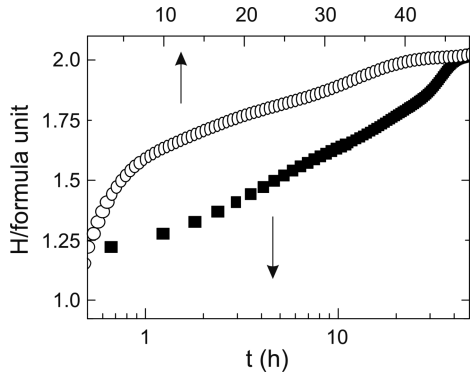

Figure 2. Hydrogen absorption behavior of NdGa at 300 °C. The time axis is presented in a linear (open symbols) and logarithmic (solid symbols) scale.

after 5 min. Further hydrogenation of initially formed hydrogenous NdGa proceeded then at a much lower rate. After 5 h a composition close to 1.5 H/formula unit was reached; the fully hydrogenated phase was eventually obtained after 45 h. The fully hydrogenated phase has a composition near 2 H/formula unit. This phase, however, does not appear to be stable without external H_2 pressure. For samples of hydrogenous NdGa obtained from autoclave synthesis, the maximum H content is estimated to be around 1.7 H/formula unit.

The hydrogen absorption behavior of NdGa is clearly complex and involves intermediate phases. Intermediate phases are also apparent in desorption of hydrogenous NdGa, which takes place in two distinct steps. The TDS experiment shows peaks with maxima at ∼250 and ∼450 °C (Figure S1a). Kissinger plots using the T_{max} (T at maximal pressure) and β (heating rate) values yielded activation energies of 115 kJ/mol for the first peak and 156 kJ/mol for the second peak (Figure S1b). PXRD analysis showed that NdGa is quantitatively reformed after complete desorption.

B. Crystal Structures of NdGa and $NdGaD_{1.66}$. NdGa crystallizes with the orthorhombic space group $Cmcm$ ($Z = 4$). Both Nd and Ga atoms are situated on sites 4c (0,y,1/4). Results of the Rietveld refinement of PXRD and neutron diffraction data agree with the reported structure by Dwight et al.[4] (Tables 1–3, S3, S6). The CrB-type structure of NdGa is built from slabs of trigonal prisms of Nd atoms, which are stacked along the [010] direction (Figure 1a). Ga atoms center Nd_6 trigonal prisms and form polyanionic zigzag chains running along [001]. The distance between Ga atoms in the chain is 2.63 Å, which is typically observed for Zintl phases containing polyanions with Ga–Ga single bonds. The bond angle in the zigzag chain is 105°. From a crystal chemistry point of view, NdGa appears to follow the Zintl concept with a formal charge assignment $Nd^{3+}Ga^{3-}$ (Figure 1b).

The stacking of Nd_6 trigonal prism slabs yields an array of edge sharing tetrahedra. The center of these tetrahedra, which also corresponds to a 4c site, may be occupied by hydrogen upon interstitial hydride formation (Figure 3a). This has been observed for the hydrogenation of isostructural CaSi to CaSiH,[18,19] and is indeed also extracted from the neutron powder diffraction data of hydrogenous NdGa. In the following, this position is denoted as H1. When fully occupied, a hydride with the composition NdGaH results. The incorporation of additional H is suggested by the kinetic absorption experiment discussed above. Difference Fourier maps revealed the presence

Table 1. Crystallographic Data and Structure Refinement for NdGa and $NdGaD_{1.66}$ from Neutron Powder Diffraction Data[a]

	empirical formula		
	NdGa	$NdGaD_{1.66}$	
space group	$Cmcm$	$Cmcm$	$P2_1/m$
unit cell (Å, deg)	a = 4.4306(3)	a = 4.1106(7)	a = 4.1103(7)
	b = 11.2478(8)	b = 12.253(2)	b = 4.1662(7)
	c = 4.1806(3)	c = 4.1665(8)	c = 6.4641(11)
			β = 108.61(1)
Z	4	4	2
V (Å^3)	208.34(3)	209.85(6)	104.9(4)
R_f	6.63	7.72	7.59
R_{wp}	4.59	5.12	5.19

[a] T = 295 K.

Table 2. Atomic Parameters of $NdGaD_{1.66}$[a]

atom	Wyck.	x	y	z	occ.	$U_{iso\ eq}$/Å^2
Nd	2e	0.344(2)	1/4	0.6880(8)	1	0.006(2)
Ga	2e	0.094(2)	1/4	0.1236(8)	1	0.0118(2)
D1	2e	0.758(3)	1/4	0.4977(8)	1	0.021(2)
D2	2e	0.56(1)	1/4	0.090(3)	0.66(2)	0.067(7)

[a] Space group $P2_1/m$.

DOI: 10.1021/acs.inorgchem.5b02485
Inorg. Chem. 2016, 55, 345–352

Table 3. Relevant Interatomic Distances (Å) and Angles (deg) in NdGa and $NdGaD_{1.66}$

NdGa							
atom1		atom2		mult.		d_{12}	
Ga		Ga		2×		2.635(3)	
angle Ga−Ga−Ga		105.00(9)					
$NdGaD_{1.66}$							
atom1	atom2	mult.	d_{12}	atom1	atom2	mult.	d_{12}
Nd	D1	1×	2.33(1)	D1	Nd	1×	2.33(1)
	D1	2×	2.374(3)		Nd	2×	2.374(3)
	D1	1×	2.40(1)		Nd	1×	2.40(1)
	D2	1×	2.46(2)		D2	1×	2.50(2)
	D2	2×	2.49(1)				
Ga	D2	1×	2.01(5)	D2	Ga	1×	2.01(5)
	D2	1×	2.12(5)		Ga	1×	2.12(5)
	Ga	2×	2.589(4)		D2	2×	2.36(1)
	D1	1×	3.01(1)		Nd	1×	2.46(2)
					Nd	2×	2.49(1)
					D1	1×	2.50(2)
angle Ga−Ga−Ga	107.1(3)						

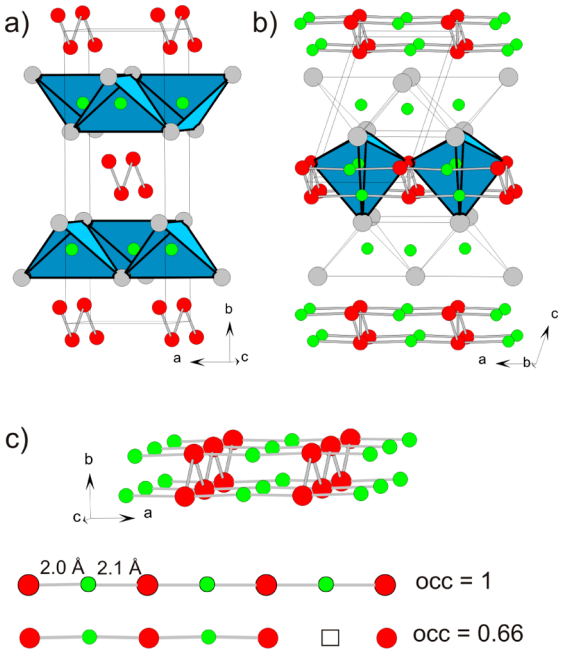

Figure 3. (a) The crystal structure of hypothetical NdGaH1. Stacking of slabs of Nd_6 trigonal prisms (cf., Figure 1a) in NdGa produces layers of edge sharing tetrahedra (blue color) as interface. Centering of tetrahedra by H yields the interstitial hydride NdGaH1. (b) The crystal structure of $NdGaD_{1.66}$. Additional H atoms (H2) are inserted between Ga atoms. The trigonal bipyramidal environment of Ga by 3 Nd and 2 H2 is highlighted (blue) for two Ga atoms. (c) Structural moiety built of Ga and H2 type atoms in $NdGaD_{1.66}$ containing quasi linear chains −Ga−H2− with two different Ga−H distances. The partial occupancy of the H2 position is demonstrated as fragmented chain. Gray, red, and green spheres denote Nd, Ga, and H(D) atoms, respectively.

of additional H atoms between Ga atoms of neighboring chains. Within the space group *Cmcm*, best fits to the neutron powder diffraction data were obtained when situating this kind of H atom (in the following denoted as H2) on a position 8g (for details, see the Supporting Information). To avoid abnormally short H2−H2 distances, this position can only be half occupied at most. The refined occupancy was then considerably lower, about 0.28 (cf., Table S4). At this point, it was concluded that hydrogenous NdGa is best expressed as $NdGaH_{1+x}$, which assumes a fully occupied site for interstitial H1 and a deficient site for H2. Lowering symmetry by using the monoclinic space group $P2_1/m$ (and $Z = 2$) allows a physically better description of H2 (Figure 3b). The refined occupancy for the H2 position then yields a composition $NdGaD_{1.66}$. Note that this is not an accurate value; rather the H content of the investigated sample should be considered between 1.6 and 1.7 H/formula unit. Nevertheless, the phase is termed as $NdGaH_{1.66}/D_{1.66}$ in the following. The refinement results are presented in Tables 1−3. The Rietveld fit to the diffraction data is shown in Figure S2. Details concerning the refinement of NdGa and $NdGaD_{1.66}$ are given as Supporting Information (Figure S2, Tables S1−S8). From the close similarity of the lattice parameters of $NdGaD_{1.66}$ and $NdGaH_x$ obtained after equilibrating NdGa in a 20 bar hydrogen atmosphere at 300 °C for 48 h, we concluded that full occupancy of the H2 position cannot be maintained without external hydrogen pressure; that is, $NdGaH_2$ is not stable under ambient pressure and temperature conditions.

Interstitial hydrogen in Zintl phases typically behaves hydridic, thus causing oxidation of the polyanion. The zigzag chain formed by Ga atoms is maintained in the hydride. The Ga−Ga distance appears reduced (from 2.63 to 2.59 Å) and the bond angle slightly widened (to 107°). This observation may indicate a change toward a π-bonded chain, thus conforming oxidation. As a consequence, the *c* axis of NdGa and $NdGaH_{1.66}$, which is the direction of the chains, is very similar. The (orthorhombic) *b* axis of $NdGaH_{1.66}$ is increased and the *a* axis decreased. The unit cell volume increase upon hydrogen incorporation is very modest.

The incorporation of a second kind of H (i.e., H2) is surprising. H2 atoms attain a trigonal bipyramidal coordination by centering a triangle of Nd atoms and bridging two Ga atoms (Figure 3b). Ga and H2 atoms are then arranged as quasi linear chains running along the [100] direction (Figure 3c). H2 deficiency in $NdGaD_{1.66}$ may be interpreted with the absence of every third H atom in a −Ga−H2− chain. Ga−H2 distances are alternating short and long, ∼2 and ∼2.1 Å. These distances are considerably longer than a Ga−H distance corresponding to a terminal bond in polyanionic hydrides (e.g., 1.69 Å in

DOI: 10.1021/acs.inorgchem.5b02485
Inorg. Chem. 2016, 55, 345−352

$SrGa_2H_2$[34] or 1.67 Å in $RbGaH_2$[35]). However, it is too short to be considered noninteracting.

C. H-Induced Structural Changes and Energetics of H Incorporation. Computational modeling of the structures of NdGaH and $NdGaH_2$ allows separating the response of the polyanionic zigzag chain to interstitial hydrogen (H1) incorporation from structural changes possibly introduced by interaction with H2 (Table 4). First, we note that the *Cmcm*

Table 4. DFT Optimized Structure Parameters and Interatomic Distances

NdGa	a = 4.4625 Å	Ga−Ga = 2.640 Å
Cmcm	b = 11.3735 Å	Ga−Ga−Ga = 105.0°
	c = 4.1885 Å	
	V = 212.6 Å^3	
NdGaH	a = 4.2211 Å	Ga−Ga = 2.51 Å
Cmcm	b = 12.0192 Å	Ga−Ga−Ga = 113.6°
	c = 4.2013 Å	
	V = 213.2 Å^3	
$NdGaH_2$	a = 4.2365 Å	Ga−Ga = 2.572 Å
$P2_1/m$	b = 4.1709 Å	Ga−Ga−Ga = 108.4°
	c = 6.4533 Å	Ga−H = 1.81, 2.43 Å
	β = 108.9°	
	$2 \times V$ = 215.7 Å^3	

structure of NdGa is excellently reproduced by DFT structure optimization (cf., Tables 1, 3). The transition from NdGa to NdGaH is accompanied by a pronounced shortening of the Ga−Ga distance (from 2.65 to 2.51 Å) and widening of the Ga−Ga−Ga angle (from 105° to 114°). At the same time, the volume increase by hydrogen incorporation is minute, 0.2 Å^3/H atom. Interestingly, when going from NdGaH to $NdGaH_2$ the Ga−Ga distance increases and the Ga−Ga−Ga angle decreases again. Also, this process is accompanied by only a small volume increase (0.6 Å^3/H atom). The volumetric hydrogen density for calculated $NdGaH_2$ is 0.04 H/Å^3, and the gravimetric density is 0.93 wt %.

The interesting feature of $NdGaH_2$ is the linear chain-like arrangement of Ga and H2 atoms. Figure 4 displays the DFT optimized structures of $NdGaH_2$ in various cells and symmetries. Within the space group (*Cmcm*) and the unit cell of the CrB type parent structure (Z = 4), H2 atoms can only be placed equidistantly between two Ga atoms (Figure 4a). Lowering symmetry to *Ama*2 allows for two different Ga−H2 distances (1.8 and 2.4 A) when displacing H2 atoms in the same direction along −Ga−H2− chains ("in-phase" displacement, cf., Figure 4b). This distortion leads to a stabilization by 0.01 eV per formula unit. Displacing H2 atoms in neighboring −Ga−H2− chains alternating in both directions ("out-of-phase", cf., Figure 4c) lowers symmetry to monoclinic. The $P2_1/m$ arrangement shown in Figure 4c, which corresponds to that assumed for the experimental structure of $NdGaD_{1.66}$, is slightly more stable than the in-phase displacement. Additional structural flexibility is provided when describing $NdGaH_2$ in a 3×a supercell, as shown in Figure 4d. Overall the most stable arrangement corresponds again to the out-of-phase displacement, but stabilization with respect to the *Cmcm* model is 0.015 eV per formula unit. The salient result of the DFT modeling of $NdGaH_2$ structures is a pronounced tendency of the −Ga−H− chain to distort and to express two different Ga−H2 distances, which are near 1.8 and 2.4 Å. This distortion is also noticeable

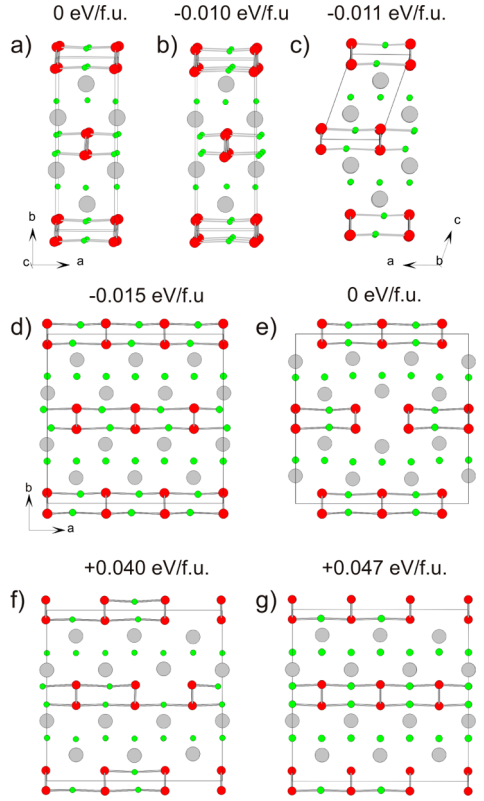

Figure 4. (a−d) DFT optimized structures for $NdGaH_2$. (a) Z = 4 cell, *Cmcm*, Ga−H = 2.09 Å (2×). (b) Z = 4 cell, *Ama*2, Ga−H = 1.82, 2.44 Å. (c) Z = 4 cell, $P2_1/m$, Ga−H = 1.81, 2.43 Å. (d) Z = 12 cell, $P2_1/m$, Ga−H = 1.82, 2.41 Å. The numbers are relative energies per formula unit with respect to structure (a). (e−g) DFT optimized structures for $NdGaH_{1.66}$, Z = 12 cells. (e) Lowest energy structure, *Cmcm*, 5-atom fragments Ga−H2−Ga−H2−Ga, Ga−H = 1.90, 2.45 Å. (f) *Pm*, chains (Ga−H = 2.05, 2.11 Å), 3-atom fragments (Ga−H = 2.16, 2.18 Å), 5-atom fragments (Ga−H = 1.86−1.91 Å, 2.31−2.40 Å). (g) *Pm*, chains (Ga−H = 2.09 (2×)), 5-atom fragments (Ga−H = 2.05, 2.15 Å). The numbers are relative energies per formula unit with respect to structure (e). Gray, red, and green spheres denote Nd, Ga, and H atoms, respectively.

in the experimental structure of $NdGaD_{1.66}$, but its extent is considerably less prominent.

It is clear that the occupation of the H1 position is preferred over the H2 one and thus will represent the first step in the hydrogenation of NdGa. Calculated energies for the reactions NdGa + 1/2 H_2 = NdGaH1 and NdGa + 1/2H_2 = NdGaH2 are −0.76 and −0.35 eV per formula unit, respectively. The calculated formation energy NdGaH1 + 1/2H_2 = $NdGaH_2$ is −0.19 eV. The energy of formation of $NdGaH_{1+x}$ according to NdGa + (x + 1)/2H_2 is shown in Figure 5. Upon filling the H2 position (i.e., for 1 < x ≤ 2), its magnitude decreases in a linear fashion with increasing x. Intermediate hydrides were simulated by model structures using a 3×a supercell containing 12 formula units. Figure 4e shows the most stable structural arrangement for $NdGaH_{1.66}$. Linear chains in $NdGaH_2$ become 5-atom fragments Ga−H2−Ga−H2−Ga in $NdGaH_{1.66}$. Interestingly, the two distinctly different Ga−H distances are maintained and for this model are around 1.9 and 2.44 Å. This is clearly not reconciled in the experimental structure of $NdGaD_{1.66}$. A likely explanation is the presence of more complex disorder in $NdGaD_{1.66}$, for example, the occurrence of larger and smaller chain fragments, as well as nonfragmented

DOI: 10.1021/acs.inorgchem.5b02485
Inorg. Chem. 2016, 55, 345−352

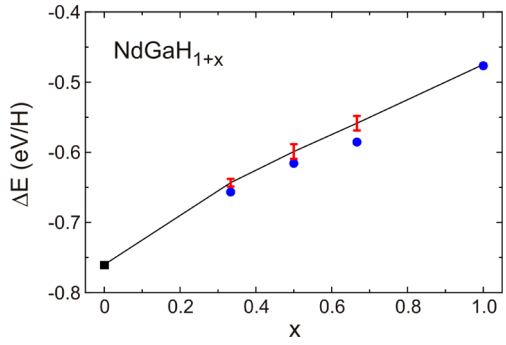

Figure 5. Energies of formation NdGa + $(x + 1)/2$ H_2 = $NdGaH_{1+x}$ as a function of x. x = 0 corresponds to NdGaH1 (Z = 4 cell). x = 0.33, 0.5, 0.66, 1.0 represent results from 3×a supercell (Z = 12) calculations. The line connects average values from 50 random starting configurations, and the red bars indicate the standard deviation. Blue symbols represent the obtained lowest energy values.

Ga−H chains alternating with rows of Ga atoms void of H. Such disorder is strongly indicated when analyzing computationally relaxed structures that yielded higher energies (Figure 4f and g). For those, a wider variety of Ga−H distances occurs. Notably, the preferred Ga−H distance within 3-atom fragments is in the range 2.0−2.1 Å.

D. H-Induced Electronic Structure Changes. The H-induced structural changes in Zintl phases can often be rationalized within the simple picture of the Zintl concept. We first consider the step from NdGa to NdGaH1 leading to an interstitial hydride (i.e., with hydridic H). Provided that an ionic description $Nd^{3+}Ga^{3-}$ is valid, charge neutrality will require that singly bonded Ga^{3-} species in the chains are oxidized to Ga^{2-}, which may then allow for π-bonding along the chain. Alternatively, because of the magnetism of NdGa, Nd and Ga may be considered as +3/−2 ions. The incorporation of hydridic hydrogen can then resolve the electronic imbalance. The calculated Bader charges (shown in Table 5) suggest that,

Table 5. Bader Charges for Atoms in NdGa, NdGaH1, and $NdGaH_2$

	Nd	Ga	H1	H2
NdGa	1.0394	−1.0394		
NdGaH1	1.4589	−0.7929	−0.6659	
$NdGaH_2$	1.5390	−0.3789	−0.6461	−0.5139

with respect to NdGa, the charge introduced by H1 in NdGaH1 is balanced by both an increase of the positive charge of Nd and a decrease of the negative charge of Ga. Independent of the Zintl oxidation state of Ga in NdGa, the resulting ionic picture for NdGaH1 is $[Nd^{3+}(H^-)Ga^{2-})]$. Comparison of the DFT optimized structures of NdGa and NdGaH1 (cf., Table 4) suggests that bonding in the polyanionic zigzag chain changed from single bonded to π-bonded.

Building on this simplified description, H2 atoms will then be located between Ga entities being part of π-bonded zigzag chains. Provided there is Ga−H2 interaction, a 2D polyanion emerges. Intuitively, Ga−H2 interaction has to be carried by the p orbitals oriented toward H, which in turn would imply the loss of π-bonding within the zigzag chain. The resulting band is composed from one orbital per atom (p_x from Ga^{2-} and s from H), which is half filled (one electron is provided from each Ga and H atom). The linear −Ga−H− chain in $NdGaH_2$ would then correspond to a classic Peierls chain, which stabilizes upon distortion (short−long distance pattern). Again, this simple picture is supported by the DFT optimized structure of $NdGaH_2$ (cf., Table 4), indicating the loss of π bonding and substantial Ga−H interaction. The Bader charge of H2 (−0.51) is considerably lower than that of H1 (−0.65), cf., Table 5. The latter appears unchanged as compared to NdGaH1. The charge introduced by H2 is mainly balanced by a reduced charge for Ga. Also, this hints to a covalent bonding interaction Ga−H2, whereas H1 remains hydridic.

Figure 6a compares the electronic density of state (DOS) for the DFT optimized structures of NdGa, NdGaH1, and

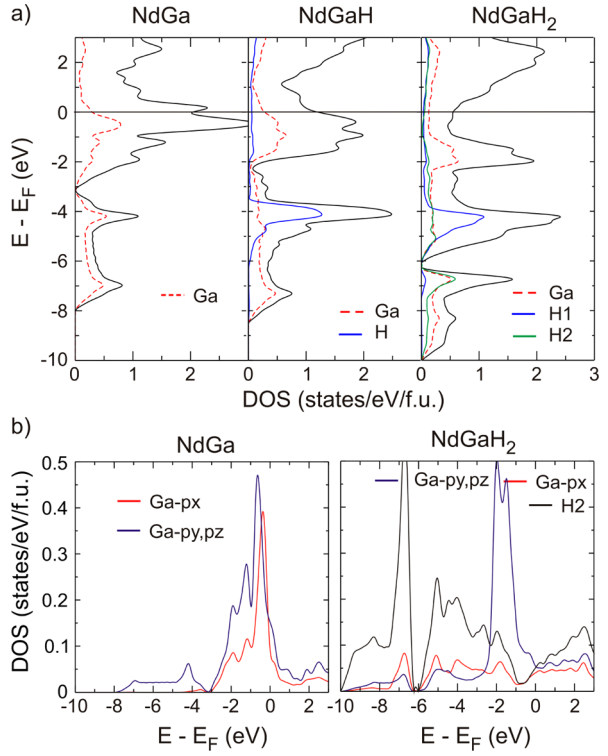

Figure 6. (a) Electronic density of states (DOS) for NdGa, NdGaH1, and $NdGaH_2$ with partial contributions of Ga, H1, and H2. (b) Partial DOS for Ga p_x, Ga p_y+p_z, and H2 for NdGa and $NdGaH_2$.

$NdGaH_2$. The DOS around the Fermi level changes largely when going from NdGa (nonmagnetic) to NdGaH to $NdGaH_2$. For $NdGaH_2$, the Fermi level is located in a broad pseudo gap, a situation typical of electron precise Zintl phases. The contribution of H1 to the DOS is seen near −4 eV below the Fermi level. The spike-like shape indicates weakly dispersed bands, which matches a hydridic nature. The contribution of Ga to the occupied states is very similar for NdGa and NdGaH1: Ga-s states contribute to bands in the region −8 to −3 eV; bands with major Ga-p contribution are located in the range −3 to 1 eV. σ-type Ga-p_y and p_z bands hybridize with Ga-s bands. The incorporation of H2 then induces drastic changes in the electronic structure. A pseudo gap is opened in the DOS at −6 eV below the Fermi level, which is flanked by spikes with large contribution of H2. In contrast to the localized contribution of H1 to the DOS, the one for H2 is distributed over a broad energy range. The shape of the partial DOS of H2 is mirrored by the partial DOS of Ga-p_x, which is changed radically as compared to NdGa and NdGaH1 (Figure 6b). This implies that states of H2, Ga-p_x, and also Ga-s contribute to the same

DOI: 10.1021/acs.inorgchem.5b02485
Inorg. Chem. 2016, 55, 345−352

bands and these bands express Ga−H2 interaction. The partial DOS of Ga-p_y and p_z are only weakly affected when going from NdGaH1 to $NdGaH_2$. One notices, however, that the tail extending above the Fermi level in NdGa and NdGaH1 is moved below the Fermi level in $NdGaH_2$. From the analysis, its DOS $NdGaH_2$ is interpreted as an electron precise Zintl phase, $Nd^{3+}(H1^-)[GaH2]^{2-}$, consequently possessing an electron precise 2D polyanion $[GaH]^{2-}$. The structure of 2D $[GaH]^{2-}$ and its bonding picture derived from a Peierls chain is a new feature in metal hydride chemistry.

E. H-Induced Magnetic Property Changes. NdGa is known to be ferromagnetic with a reported $T_C \approx 45$ K.[13−16] A similar behavior is seen in our sample, as shown in Figure 7a

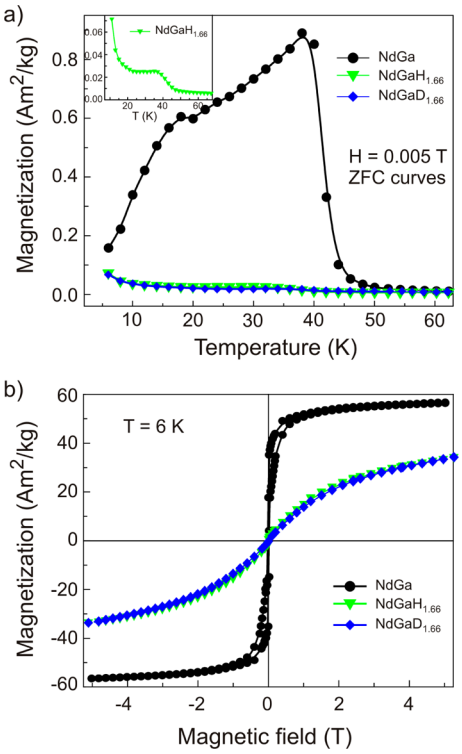

Figure 7. (a) Zero field cooled M versus T curves of $NdGa(H/D)_{1.66}$ at $H = 0.005$ T. (b) Isothermal magnetization curves of $NdGa(H/D)_{1.66}$ recorded at $T = 6$ K.

(black curve). This figure contains the zero field cooled (ZFC) M versus T curves of NdGa, $NdGaH_{1.66}$, and $NdGaD_{1.66}$ recorded under a magnetic field of 0.005 T. It is seen that hydrogen incorporation effectively suppresses the ferromagnetism. Nevertheless, the ferromagnetic transition of NdGa is still remanent in $NdGaH_{1.66}$ and $NdGaD_{1.66}$, and can be seen as a small increase in the magnetization when the sample is cooled below 40 K (see inset of Figure 7a). Figure 7b displays the low temperature ($T = 6$ K) M versus H behavior of the samples. For NdGa (black curve), the magnetization increases rapidly for low values of the magnetic field, and reaches a saturation value of ~55 Am^2/kg. For $NdGaH_{1.66}$ and $NdGaD_{1.66}$, the curves do not display a ferromagnetic nature. The magnetization shows a more gradual increase with the applied magnetic field, and saturation is not obtained (green and blue curves).

M versus T curves were also recorded at a higher applied magnetic field, $H = 0.1$ T (data not shown here), to make Curie−Weiss fits to the high temperature susceptibility data ($\chi = C/(T - \theta_{CW})$). The extracted values of the effective magnetic moment (μ_{eff}) and the Curie−Weiss constant (θ_{CW}) are given in Table 6. The μ_{eff} values obtained from the fits are close to the

Table 6. Effective Magnetic Moments (μ_{eff}) and Curie−Weiss Constants (θ_{CW}) Obtained from Curie−Weiss Fits to the High Temperature Susceptibility Data

sample	μ_{eff} (μ_B)	θ_{CW} (K)
NdGa	3.33	32.7
$NdGaH_{1.66}$	3.68	−23.1
$NdGaD_{1.66}$	3.60	−22.4

theoretical value for Nd^{3+} with three unpaired electrons (3.62 μ_B). For NdGa a positive value of the Curie−Weiss constant (θ_{CW}) was obtained, which is rather close to the ferromagnetic T_C of the sample, thereby indicating the presence of expected ferromagnetic correlations. Notably, for $NdGaH_{1.66}$, the value of θ_{CW} is negative. Thus, the incorporation of hydrogen alters the exchange interaction from ferromagnetic to antiferromagnetic. Despite this general tendency yielding a change of sign of the Nd−Nd interaction, there remain local ferromagnetic regions indicating an inhomogeneous distribution of hydrogen in $NdGaH_{1.66}$ samples.

IV. CONCLUSIONS

NdGa absorbs hydrogen reversibly to yield $NdGaH_{1+x}$. H incorporates in NdGa by occupying two distinct positions, H1 and H2. H1 is exclusively coordinated by Nd atoms in a tetrahedral fashion and thereby of hydridic (H^-) nature. The H2 position displays flexible occupancy, and H2 atoms attain a trigonal bipyramidal coordination by centering a triangle of Nd atoms and bridging two Ga atoms. Fully hydrogenated $NdGaH_2$ ($x = 1$) is considered an electron precise Zintl phase $Nd^{3+}(H1^-)[GaH2]^{2-}$. The two-dimensional polyanion $[GaH]^{2-}$ features novel linear −H−Ga−H−Ga− chains with alternating short and long Ga−H distances, which resembles a Peierls distortion. H2 deficiency ($x < 1$) results in the fragmentation of chains. In contrast with NdGa, $NdGaH_{1+x}$ does not show ferromagnetic coupling. The effective magnetic moment of here investigated $NdGaH_{1.66}$ is close to that of NdGa above T_C, indicating that Nd possesses the same oxidation state (+3) in both systems.

The peculiar feature of hydrogenous Zintl phases is the coexistence of hydrogen and polymeric anions composed of p-block atoms. It is noteworthy that $NdGaH_{1+x}$ contains both interstitial H (H1) and H being part of the polyanion (H2). This has been observed earlier only for $Rb_8Ga_5H_{15}$ and $Cs_{10}Ga_9H_{25}$.[35,36] Furthermore, fully hydrogenated $NdGaH_2$ may only exist in the presence of pressurized hydrogen. Recently, Wenderoth and Kohlmann showed the impressive potential of in situ neutron powder diffraction for studying hydrogenation processes of Zintl phases.[37] It will be very interesting to perform time-resolved structural studies also for NdGa, to reveal the different stages in the evolution of $[GaH]^{2-}$ chains and their completion in fully hydrogenated $NdGaH_2$.

■ ASSOCIATED CONTENT

Supporting Information

The Supporting Information is available free of charge on the ACS Publications website at DOI: 10.1021/acs.inorgchem.5b02485.

Thermal desorption mass spectroscopy curves of $NdGaD_{1.66}$ and evaluation of activation energies (Figure

DOI: 10.1021/acs.inorgchem.5b02485
Inorg. Chem. 2016, 55, 345−352

S1); Rietveld fits to the neutron diffraction patterns of NdGa, $NdGaD_{1.66}$ (*Cmcm*), and $NdGaD_{1.66}$ ($P2_1/m$) (Figure S2); refinement parameters (Table S1), compilation of unit cell parameters (Table S2), atomic parameters of NdGa (Tables S3), atomic parameters of $NdGaD_{1.66}$ (*Cmcm*) (Table S4), atomic parameters of $NdGaD_{1.66}$ ($P2_1/m$) (Table S5), interatomic distances for NdGa (Table S6), interatomic distances for $NdGaD_{1.66}$ (*Cmcm*) (Table S7), and interatomic distances for $NdGaD_{1.66}$ ($P2_1/m$) (Table S8) (PDF)
X-ray data for $NdGaD_{1.66}$ (CIF)

AUTHOR INFORMATION

Corresponding Author

*E-mail: ulrich.haussermann@mmk.su.se.

Notes

The authors declare no competing financial interest.

ACKNOWLEDGMENTS

We would like to thank Mr. Maciek Kaplan for synthesis of the NdGa sample and Dr. Ceasar Pay Gómez for help with Fourier maps. Access to beam times at the JEEPII reactor of Institute for Energy Technology via the FP7 Research Infrastructure H2FC (Grant agreement no. 284522) is gratefully acknowledged. Financial support from the Swedish Research Council is also acknowledged.

REFERENCES

(1) Häussermann, U.; Kranak, V. F.; Puhakainen, K. Hydrogenous Zintl Phases: Interstitial Versus Polyanionic Hydrides. In *Zintl Phases: Principles and Recent Developments*; Fässler, T. F., Ed.; Structure and Bonding; Springer: Berlin, Germany, 2011; Vol. *139*, pp 143−161.
(2) Häussermann, U. *Z. Kristallogr.* **2008**, *223*, 628−635.
(3) Schob, O.; Parthé, E. *Acta Crystallogr.* **1965**, *19*, 214−224.
(4) Dwight, A. E.; Downey, J. W.; Conner, R. A., Jnr *Acta Crystallogr.* **1967**, *23*, 860−862.
(5) Villars, P.; Calvert, L. D. *Pearson's Handbook of Crystallographic Data for Intermetallic Compounds*, 2nd ed.; ASM International: Materials Park, OH, 1991; and desk ed., 1997.
(6) Zhang, J. Y.; Luo, J.; Li, J. B.; Liang, J. K.; Wang, Y. C.; Ji, L. N.; Liu, Y. H.; Rao, G. H. *J. Alloys Compd.* **2009**, *469*, 15−19.
(7) Chen, J.; Shen, B. G.; Dong, Q. Y.; Hu, F. X.; Sun, J. R. *Appl. Phys. Lett.* **2009**, *95*, 132504.
(8) Chen, J.; Shen, B. G.; Dong, Q. Y.; Sun, J. R. *Solid State Commun.* **2010**, *150*, 157−159.
(9) Zheng, X. Q.; Chen, J.; Shen, J.; Zhang, H.; Xu, Z. Y.; Gao, W. W.; Wu, J. F.; Hu, F. X.; Sun, J. R.; Shen, B. G. *J. Appl. Phys.* **2012**, *111*, 07A917.
(10) Gao, T.; Nishimura, K.; Matsumoto, T.; Namiki, T.; Isikawa, Y. *Solid State Commun.* **2013**, *158*, 1−4.
(11) Mo, Z. J.; Shen, J.; Yan, L. Q.; Tang, C. C.; Lin, J.; Wu, J. F.; Sun, J. R.; Wang, L. C.; Zheng, X. Q.; Shen, B. G. *Appl. Phys. Lett.* **2013**, *103*, 052409.
(12) Barbara, B.; Nyugen, V. N.; Siaud, E. *C. R. Acad. Sci. B* **1972**, *274*, 1053−1056.
(13) Fujii, H.; Shohata, N.; Okamoto, T.; Tatsumoto, E. *J. Phys. Soc. Jpn.* **1971**, *31*, 1592.
(14) Shohata, N. *J. Phys. Soc. Jpn.* **1977**, *42*, 1873−1880.
(15) Grin, Y.; Sichevich, O. M.; Hiebl, K. *IEEE Trans. Magn.* **1994**, *30*, 4975−4977.
(16) Delyagin, N. N.; Krylov, V. I.; Rozantsev, I. N. *J. Magn. Magn. Mater.* **2007**, *308*, 74−79.
(17) Aoki, M.; Ohba, N.; Noritake, T.; Towata, S. *Appl. Phys. Lett.* **2004**, *85*, 387−388.
(18) Ohba, N.; Aoki, M.; Noritake, T.; Miwa, K.; Towata, S. *Phys. Rev. B: Condens. Matter Mater. Phys.* **2005**, *72*, 075104.
(19) Wu, H.; Zhou, W.; Udovic, T. J.; Rush, J. J.; Yildirim, T. *Phys. Rev. B: Condens. Matter Mater. Phys.* **2006**, *74*, 224101.
(20) BeN Systems. Computer program "UnitCell version 1", 2000.
(21) Hauback, B. C.; Fjellvåg, H.; Steinsvoll, O.; Johansson, K.; Buset, O. T.; Jørgensen, J. *J. Neutron Res.* **2000**, *8*, 215−232.
(22) (a) Rodriguez-Carvajal, J. *FullProf 2.k, version 5.20*; ILL: Grenoble, France, 2011. Rodríguez-Carvajal, J. *Abstracts of the Satellite Meeting on Powder Diffraction of the XV IUCr Congress* **1990**, 127. (b) Rodriguez-Carvajal, J. *Int. Union Crystallogr. Newsl.* **2001**, *26*, 12−19.
(23) González-Platas, J.; Rodríguez-Carvajal, J. GFourier: a Windows/Linux program to calculate and display Fourier maps. Program available within the FullProf Suite.
(24) Kissinger, H. E. *Anal. Chem.* **1957**, *29*, 1702−1706.
(25) Blöchl, P. E. *Phys. Rev. B: Condens. Matter Mater. Phys.* **1994**, *50*, 17953−17979.
(26) Kresse, G.; Joubert, D. *Phys. Rev. B: Condens. Matter Mater. Phys.* **1999**, *59*, 1758−1775.
(27) (a) Kresse, G.; Hafner, J. *Phys. Rev. B: Condens. Matter Mater. Phys.* **1993**, *47*, 558−561. (b) Kresse, G.; Hafner, J. *Phys. Rev. B: Condens. Matter Mater. Phys.* **1994**, *49*, 14251−14269.
(28) (a) Kresse, G.; Furthmüller, J. *Comput. Mater. Sci.* **1996**, *6*, 15−50. (b) Kresse, G.; Furthmüller, J. *Phys. Rev. B: Condens. Matter Mater. Phys.* **1996**, *54*, 11169−11186.
(29) (a) Perdew, J. P.; Burke, K.; Ernzerhof, M. *Phys. Rev. Lett.* **1996**, *77*, 3865−3868. (b) Perdew, J. P.; Burke, K.; Ernzerhof, M. *Phys. Rev. Lett.* **1997**, *78*, 1396.
(30) Stokes, H. T.; Hatch, D. M. *J. Appl. Crystallogr.* **2005**, *38*, 237−238.
(31) Monkhorst, H. J.; Pack, J. D. *Phys. Rev. B* **1976**, *13*, 5188−5192.
(32) Bader, R. F. W. *Atoms in Molecules: A Quantum Theory*; Oxford University Press: Oxford, 1990; pp 1−52.
(33) (a) Armaldsen, A.; Tang, W.; Henkelman, G., http://theory.cm.utexas.edu/bader/. (b) Tang, W.; Sanville, E.; Henkelman, G. *J. Phys.: Condens. Matter* **2009**, *21*, 084204.
(34) Björling, T.; Noréus, D.; Häussermann, U. *J. Am. Chem. Soc.* **2006**, *128*, 817−824.
(35) Fahlquist, H.; Noréus, D.; Callear, S.; David, W. I. F.; Hauback, B. C. *J. Am. Chem. Soc.* **2011**, *133*, 14574−14577.
(36) Fahlquist, H.; Noréus, D. *Inorg. Chem.* **2013**, *52*, 7125−7129.
(37) Wenderoth, P.; Kohlmann, H. *Inorg. Chem.* **2013**, *52*, 10525−10531.

DOI: 10.1021/acs.inorgchem.5b02485
Inorg. Chem. 2016, 55, 345−352